The Flow Past a Non-Isothermal Shrinking Sheet with the Effects of Thermal Radiation and Heat Source/Sink

N. Nithya and B. Vennila *

Abstract—**This research article explores the effect of thermal radiation and heat source/sink on a hybrid nanofluid comprising of Aluminium oxide (Al_2O_3) and Titanium dioxide (TiO2) nanoparticles suspended in the base fluid of water (H_2O). The bvp4c algorithm is utilized to solve the governing equations, and the influence of various parameters on velocity and temperature is examined via graphs. It is noted that the magnetic parameter (M) escalates the temperature and increases penetrates the velocity. In addition, the skin friction and heat transfer effects are also discussed**

Index Terms—**radiative heat, heat source/sink, skin friction, nusselt number, magnetic.**

I. Introduction

A substance that concurrently combines the physical and chemical characteristics of various materials is called a hybrid material. Numerous studies have been conducted by many researchers to study the optical, mechanical, electrical and thermal properties of these hybrid materials. A hybrid nanofluid is prepared by dispersing two different types of nanoparticles in the base fluid, this is done to obtain a wide absorption range, high thermal conductivity, lower extinction, low pressure-drop, pumping power and low frictional losses. It has crucial applications in the automotive industry, in heat pipes, as a coolant in machining processes, in solar systems, in heat exchangers, for nuclear system cooling, in electronic cooling, in the biomedical industry and in the defense field.

Magnetohydrodynamics (MHD) is the study of the impacts of a magnetic field on liquids. Such studies are important as the magnetic field exists everywhere in the universe. MHD focuses on an electrically conducting fluid that moves in a magnetic field and can be used to control the heat transfer system. The Lorentz force is created by the MHD effect, which is very useful for controlling cooling structures. Many researchers have employed MHD concepts in different industrial applications such as flow metering, nuclear trash disposal, and extracting geothermal energy. Radiative fluids are a type of fluid that emits energy in the form of radiation. These fluids are critical to the successful functioning of several industrial operations. They are particularly useful in systems with large temperature differences between the environmental fluid and the boundary externals.

Manuscript received April 29, 2023; revised October 10, 2023.

N. Nithya is a Research Scholar in the Department of Mathematics, College of Engineering and Technology, SRM Institute of Science and Technology, Kattankulathur-603 203, Tamil Nadu, India. (e-mail:nn7589@srmist.edu.in).

B. Vennila is an Associate Professor in the Department of Mathematics, College of Engineering and Technology, SRM Institute of Science and Technology, Kattankulathur-603 203, Tamil Nadu, India. (corresponding author; phone: 9445413186; email: vennilab@srmist.edu.in).

Grubka and Bobba [1] studied the heat transfer characteristics of a continuous, stretching surface with variable temperature. Merkin [2] determined the dual solutions of mixed convection flow in a porous medium. Weidman et al. [3] examined the effect of transpiration on self-similar boundary layer flow over moving surfaces. The fluid flows heat and mass transfer and the boundary layers across a sheet constantly contracting as per power law velocity were examined by Fang [4]. Tie-Gang et al.[5], Arifin et al.[6], and Rohini et al. [7] explained the viscous flow over a shrinking sheet with concentration transmission. Zaimi et al. [8] scrutinized boundary layer flow and heat transfer past a permeable shrinking sheet in a nanofluid with radiation effect. Bachok et al. [9] explained the copper-water nanofluid of stagnation-point flow over a permeable stretching/shrinking sheet. Rohini et al. [10] studied an unsteady nanofluid flow of a shrinking sheet with suction using Buongiornos model. Das [11], [12], Awati et al.[13], Hafidzuddin and Nazar [14], Ene et al. [15], and Yao et al. [16] discussed the results of an analytical and numerical study of thermal conduction and heat and mass transmission for the boundary layer flow over a permeable shrinking sheet with power law velocity. Dogonchi et al. [17] adopted an analytical method of Adomian Decomposition for continuous, viscous, incompressible water-based MHD radiative nanofluid flow between two stretchable or shrinkable walls. Das et al. [18] assessed the boundary layer flow of nanofluid over a convectively heated shrinking sheet in the presence of a thermal sink or source. The three-dimensional rotational nanofluid flow and heat transmission were explained by Hayat et al. [19]. Rashid et al. [20] determined the flow of water-based alumina and copper nanoparticles along a moving surface with variable temperature.

Abbaje et al. [21] scrutinized an incompressible unsteady Powell-Eyring nanofluid flow past a shrinking space with the squeal of thermal radiation and heat production. A multi-domain bivariate spectral quasi-linearization method was used to obtain numerical solutions for nonlinear differential equations that described the transport processes. Thumma et al. [22] used the Maxwell and Brinkman models for the numerical study of radiative hydrodynamic blended convection boundary layer flow of nanofluid across a nonlinear inclination shrinking/stretching surface with viscous dissipation and a heat source. Vajravel et al. [23] studied the MHD flow and heat transfer over a slender elastic permeable sheet in a rotating fluid with Hall current. Usman et al. [24] assessed the notable impacts of thermal conductivity varying with time and nonlinear thermal radiation caused by spinning Cu + Al_2O_3/water hybrid nanofluid flow across a three-dimensional stretched sheet. The solution of the proposed model was evaluated using the least squares method (LSM). Ghadikolaei et al. [25], [26] adopted the numerical technique (Runge-Kutta-Fehlberg) for hybrid nanofluids Al_2O_3 Cu/water and the mixture of ethylene glycol-water/TiO_2 + CuO over a porous medium and rotating cone by taking into account the form factor of the nanoparticles. Waini et al. [27] solved the problem of the unsteady flow of a hybrid nanofluid past a stretching sheet using a numerical shooting technique. Khashi et al. [28] discovered the effect of suction on the magnetic flow in double stratified micro-polar fluid across a shrinking sheet. Japili et al. [29] and Norzwary et al. [30] investigated the slip flow of MHD nanofluid past a permeable shrinking surface. Dinarvand et al. [31] studied the numerical computational of an unsteady flow towards over a shrinking or stretched sheet in porous media filled with a hybrid nanofluid. Sajjad et al. [32] investigated the thermal heat slip, joule heating, and two solution's flow of magnetohydrodynamic Al2O3 + Cu hybrid nanofluid over a vertically shrinking sheet. Waini et al. [33] and Maranna et al. [34] explained the flow of a radiative hybrid and ternary hybrid nanofluid over a shrinking sheet. Nithya and Vennila [35] examined the heat and mass transmission of two nanofluids (Ag/H_2O and Cuo/H_2O) by considering the effects of ohmic heating, viscous dissipation, thermophoresis properties, Brownian motion, and thermal radiation. Khan et al. [36] found dual solutions for radiative stagnation point flow of a hybrid nanofluid across a shrinking sheet, based on a numerical study . Visalakshi et al. [37] explained the skin friction of radiative hybrid nanofluid flow over a stretching/shrinking sheet. Nithya and Vennila [38] reported an analytical solution of mass and heat transfer of nanoliquid flow over a stretching sheet by studying the effects viscous dissipation and ohmic dissipation.

In this research article, the magnetic flow caused by a non-isothermal shrinking surface of a hybrid nanofluid ($Al_2O_3 - TiO_2/H_2O$) is presented. The obtained numerical results are discussed and showcased in tables and figures. The momentum and thermal fields are significantly influenced by the radiation, heat sink parameters, and volume fraction.

II. Mathematical Model

The two-dimensional, incompressible laminar flow of a hybrid nanofluid past a non-isothermal permeable shrinking sheet is studied by considering $Al_2O_3 - TiO_2/H2O$ with the Tiwari and Das model. The sheet velocity is obtained by $u_w(x) = bx$, where $b > 0$ is constant . The governing equation is written in the usual notation under boundary-layer approximation. The flow is affected by the combined action of a transverse magnetic field with a strength of B_0 and radiative heat with a heat flux of q_r, which is applied normally to the surface in the y-direction [33]

$$\frac{\partial u}{\partial x} + \frac{\partial v}{\partial y} = 0 \tag{1}$$

$$u\frac{\partial u}{\partial x} + v\frac{\partial u}{\partial y} = \frac{\mu_{hnf}}{\rho_{hnf}}\frac{\partial^2 u}{\partial y^2} - \frac{\sigma_{hnf}}{\varrho_{hnf}}B_0^2 u \tag{2}$$

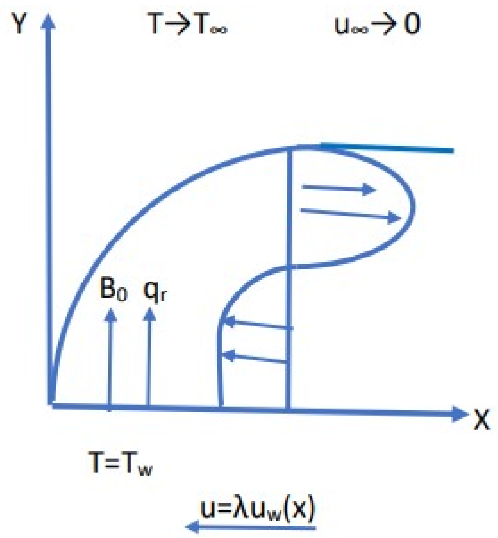

Fig. 1: Physical representation of flow model

$$u\frac{\partial \top}{\partial x} + v\frac{\partial \top}{\partial y} = \frac{K_{hnf}}{(\rho C_p)_{hnf}}\frac{\partial^2 \top}{\partial y^2} - \frac{1}{(\rho C_p)_{hnf}}\frac{\partial q_r}{\partial y} + \frac{Q_0}{(\rho C_p)_{hnf}}(\top - \top_\infty) \tag{3}$$

subject to:

$$v = v_0, u = \lambda u_w(x), \top = \top_w(x) \text{ at } y = 0 \tag{4}$$

$$u \longrightarrow 0, \top \longrightarrow \top_\infty \text{ at } y \longrightarrow \infty \tag{5}$$

The velocity components in the x and y directions are denoted by u and v respectively. Considering Rosseland's approximation for radiation as

$$q_r = -\frac{4\sigma^*}{3K^*}\frac{\partial \top^4}{\partial y} \tag{6}$$

Where, K^* and σ^* denote the mean absorption coefficient and Stefan-Boltzman constant respectively. $\top^4$ may be expressed as a temperature linear function as $\top^4 = 4\top_\infty^3$, then the following is given by equation (3).

$$u\frac{\partial \top}{\partial x} + v\frac{\partial \top}{\partial y} = \frac{1}{(\rho C_p)_{hnf}}\left\{\left[K_{hnf} + \frac{16\sigma^*\top_\infty^3}{3K^*}\right]\frac{\partial^2 \top}{\partial y^2}\right\} + \frac{1}{(\rho C_p)_{hnf}}\frac{Q_0}{(\top - \top_\infty)} \tag{7}$$

The surface temperature is as follows

$$\top_w(x) = \top_\infty + \top_0(x/L)^m \tag{8}$$

Here, $\top_0$ is the thermal variable and L is a sheet's characteristic length. The surrounding temperature $\top_\infty$ is constant and m is denoted as power-law index, with $m = 0$ specifying as isothermal sheet and $m > 0$ specifying as non-isothermal sheet

Now, adopting the similarity transformation

$$\psi = \sqrt{a\nu_f}xf(\eta),\ \theta(\eta) = \frac{\top - \top_\infty}{\top_w - \top_\infty},\ \eta = \sqrt{\frac{a}{\nu_f}} \tag{9}$$

ψ is the stream function, where $v = -\frac{\partial \psi}{\partial x}$and $u = \frac{\partial \psi}{\partial y}$, then:

$$u = axf'(\eta),\ \ v = -\sqrt{a\nu_f}f(\eta) \tag{10}$$

In equation (10), setting $\eta = 0$, we can obtain

$$v_0 = -\sqrt{a\nu_f}S \tag{11}$$

Here, the sheet's permeability is determined by the constant mass flux, $f(0) = S$. where, $S > 0$ (suction) and $S < 0$ (injection). Using the equations (9) and (10) in equations (2) and (3), we get

$$\frac{\mu_{hnf}/\mu_f}{\rho_{hnf}/\rho_f} f''' - f'^2 + ff'' - \frac{\sigma_{hnf}/\sigma_f}{\rho_{hnf}/\rho_f} Mf' = 0 \tag{12}$$

$$\frac{1}{Pr}\left[k_{hnf/kf} + \frac{4}{3}R\right]\theta'' + \frac{(\rho C_p)_{hnf}}{(\rho C_p)_f}(f\theta' - mf'\theta) + Q\theta = 0 \tag{13}$$

subject to the following

$$f(0) = S,\ f^{'}(0) = \lambda,\ \theta(0) = 1,\ \text{at}\ \eta = 0 \tag{14}$$

$$f'(\eta) \to 0,\ \theta(\eta) \to 0,\ \text{at}\ \eta \to \infty \tag{15}$$

Take into account that the indicators for a stretched surface as $\lambda > 0$ and a shrinking surface as $\lambda < 0$, where
$Pr = \frac{(\mu C_p)_f}{k_f}, R = \frac{4\sigma^* T_\infty^3}{k^* k_f}, M = \frac{\sigma_f}{\rho_f a} B_0^2$
The coefficient of the skin friction C_f and local Nusselt number Nu_x are described by

$$C_f = \frac{\mu_{hnf}}{\rho_f u_w^2}\left(\frac{\partial u}{\partial y}\right)_{y=0}$$

$$Nu_x = \frac{x}{k_f(\top_w - \top_\infty)}\left(-k_{hnf}\left(\frac{\partial \top}{\partial y}\right)_{y=0} + (q_r)_{y=0}\right)$$

using equation (8) and (13) we can obtain,

$$Re_x^{1/2} C_f = \frac{\mu_{hnf}}{\mu_f} f''(0) \tag{16}$$

$$Re_x^{-1/2} Nu_x = -\left(\frac{k_{hnf}}{k_f} + \frac{4}{3}R\right)\theta'(0) \tag{17}$$

$Re_x = u_w(x)/\nu_f$ represents the local Reynolds number

Numerical Procedure

The non linear couple ODEs (12) and (13) with boundary condition (14) and (15) and were solved using bvp4c technique. Now converting higher order non linear ordinary differential equations into system of first order ODE, by introducing new variables
$f = y(1);\ f' = y(2);\ f'' = y(3);\ \theta = y(4);\ \theta' = y(5)$

$$dy = \Bigg[y(2)$$
$$y(3)$$
$$\left(\frac{\rho_{hnf}/\rho_f}{\mu_{hnf}/\mu_f}\right) * ((y(2))^2 - y(1) * y(3) +$$
$$\left(\frac{\sigma_{hnf}/\sigma_f}{\rho_{hnf}/\rho_f}\right) * M * y(2))$$
$$y(5)$$
$$\frac{Pr}{\left(\frac{k_{hnf}}{k_f} + \frac{4}{3}R\right)} *$$
$$\left(\frac{(\rho C_p)_{hnf}}{(\rho C_p)_f}(y(1)y(5) - my(2)y(4)) - Qy(4)\right)\Bigg]$$

with boundary condition: $f(0) = ya(1) = S$;
$f'(0) = ya(2) = \lambda$; $\theta(0) = ya(4) = 1$;
$f'(\infty) = yb(2)$; $\theta(\infty) = yb(4)$

III. Result and Discussion

The effect of ϕ_1, ϕ_2 for $Al_2O_3 - TiO_2$ and S, M, m, R, Q are analysed and further discussed. Pr is taken as 6.8(water) and ϕ ranges from 0 to 0.02, where $0 \le \phi_1 \le 0.02$, $0 \le \phi_2 \le 0.022$, $1.9 \le S \le 1.7$, $0.1 \le M \le 0.3$, $1 \le m \le 2$, $5 \le R \le 6$, $0.1 \le Q \le 0.3$.

Velocity profile:

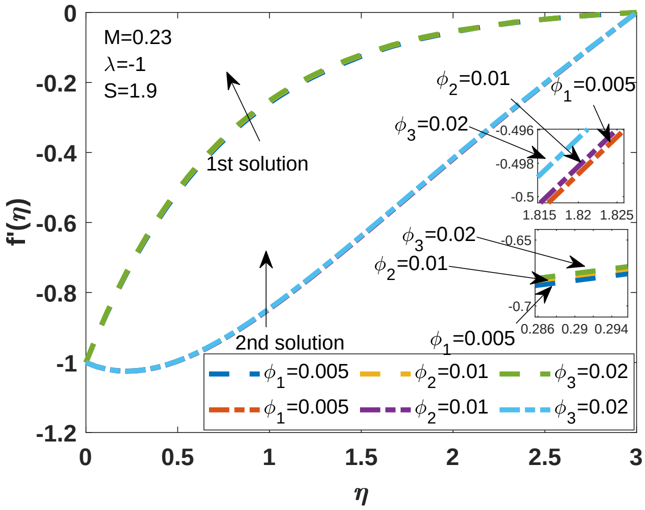

Fig. 2: The effect of ϕ_1, ϕ_2 on velocity profile

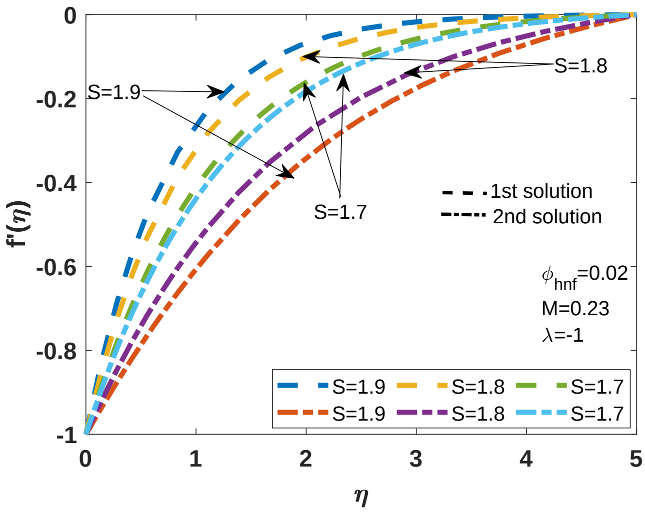

Fig. 3: The effect of S on velocity profile

Figure 2 displays the trend of the velocity distribution under the influence of volume fraction. For both solutions, it is clear that $f'(\eta)$ does not decline near the sheet as the parameter of nanoparticle volume fraction increases. This outcome demonstrates that the momentum boundary layer does not thin for the first and second solutions.
We present the velocity profile $f'(\eta)$ for several values of a permeable shrinking surface with a suction parameter in Figure 3, where the behavior of $f'(\eta)$ shows an increment

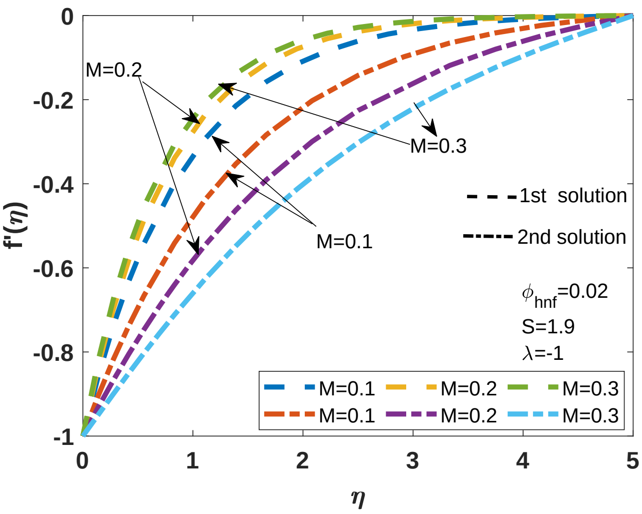

Fig. 4: The effect of M on velocity profile

in the lower solution and a decrement in the upper solution versus the decreased number of S. Physically, the variations in the suction parameter are inversely proportional to $f'(\eta)$. It is consistent with the physical reality that when S increases, the momentum boundary layer tends to adhere to the stretching sheet, disrupting the flow momentum.

In Figure 4, there is an increase in the first solution of $f'(\eta)$ as M expands the hybrid nanofluid flow. The presence of the magnetic field in an electrically conducting fluid boosts the Lorentz force, which is a resistive force. This force provides resistance in opposition to the motion of the fluid particle, lowering the fluid's velocity. The synchronization of the magnetic and electrical fields caused by the Lorentz force tends to slow the speed of the conducting fluid near the boundary layer. In short, increasing M raises $f'(\eta)$, which increases the frictional drag produced on the sheet surface. However, about the second solution in Figure 4, $f'(\eta)$ was discovered to be diminishing as M increased from 0.1 to 0.3. The velocity of the hybrid nanofluid reduces as it passes through the shrinking sheet, increasing the thickness of the momentum boundary layer. This unusual tendency could be attributed to the shrinking sheet event, which restricted the infiltration of hybrid nanofluid molecules.

Temperature profile:

Figure 5 depicts the trend of temperature distribution for solid volume fraction of hybrid nanofluid. Physically, the nanoparticles dissipate energy in the form of heat. Furthermore, we discovered that the first solution of $\theta(\eta)$ rises when the nanoparticle volume percentage increases. The higher concentration of nanoparticles improves the thermal conductivity of hybrid nanofluid. As expected, increasing thermal conductivity of the hybrid nanofluid has a positive impact on fluid temperature as the nanoparticles volume fraction grows. But, we may get a opposite result for second solution of thermal distribution.

The influence of the magnetic field coefficient on the temperature pattern is depicted graphically in Figure 6. It suggests an improvement in $\theta(\eta)$ with M. This is because the created Lorentz force (as a result of M changes) increases the friction between the fluid layers, which improves the temperature profile. it is obvious that the fluid temperature and boundary layer thickness rise with higher values of this parameter.

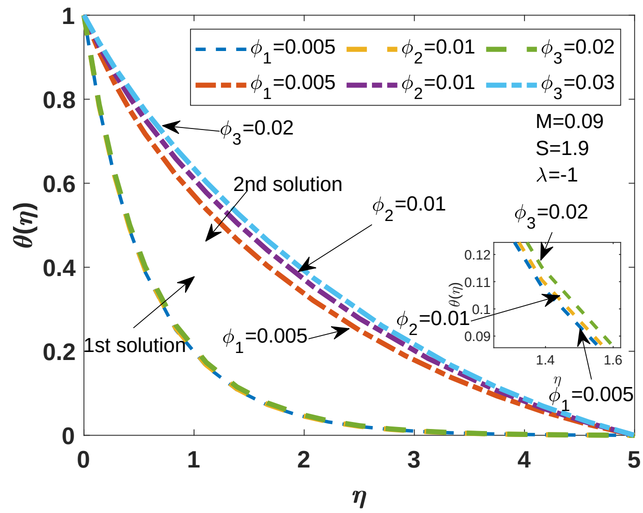

Fig. 5: The effect of ϕ_1, ϕ_2 on thermal profile

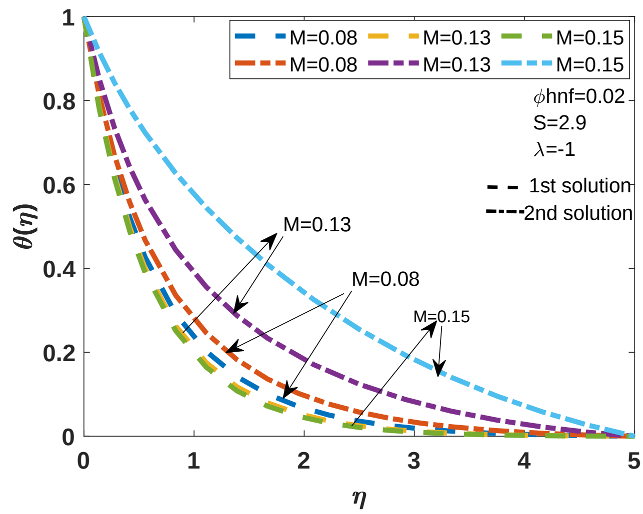

Fig. 6: The effect of M on thermal profile

Figure 7 depicts the temperature profiles behavior, when different thermal radiation parameters (R) are used. This variable occurs exclusively in the thermal Equation (13), and it is decoupled from momentum Equation (12); thus, changing the value of R has no effect on the velocity profile. The thermal boundary layer width improves with Rd in both solutions, implying that the temperature gradient at the surface is lower for larger R quantities. Physically, the radiation parameter measures the distribution of thermal radiation due to the flow of heat through conduction. Higher values of this radiation parameter thus show the dominance of thermal radiation over conduction. Therefore, a large amount of heat energy is emitted in the system due to radiation, which leads to an increase in the temperature. This indicates that the temperature of the fluid $\theta(\eta)$ increases because of the presence of high radiation. As demonstrated in Figure 8, the effect of the heat generation/absorption parameter on the fluid temperature distribution results in a substantial enhancement

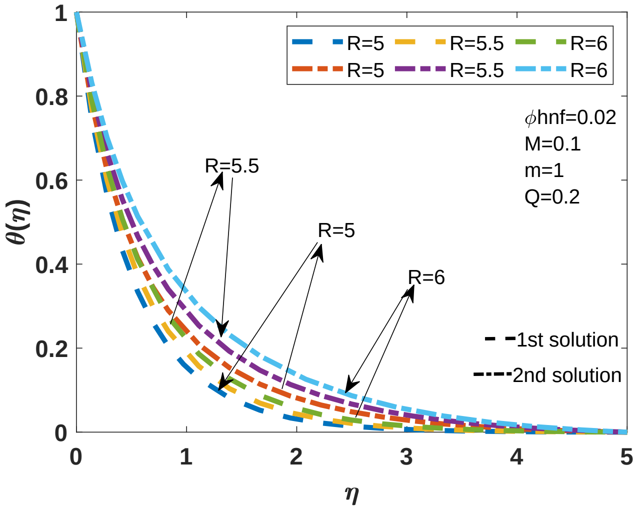

Fig. 7: The sequel of R on thermal profile

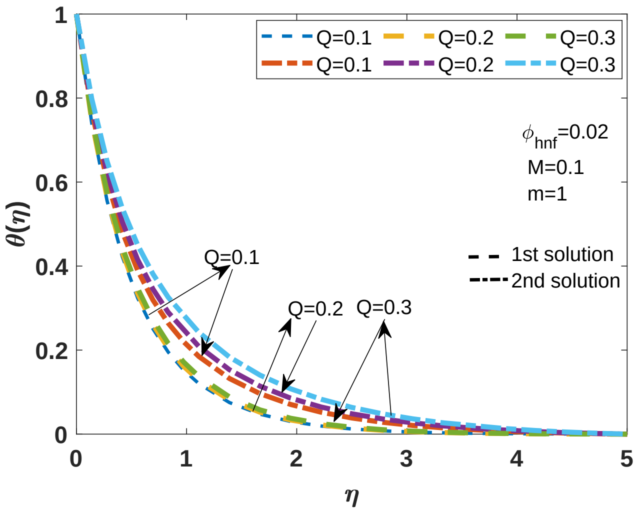

Fig. 8: The sequel of Q on thermal profile

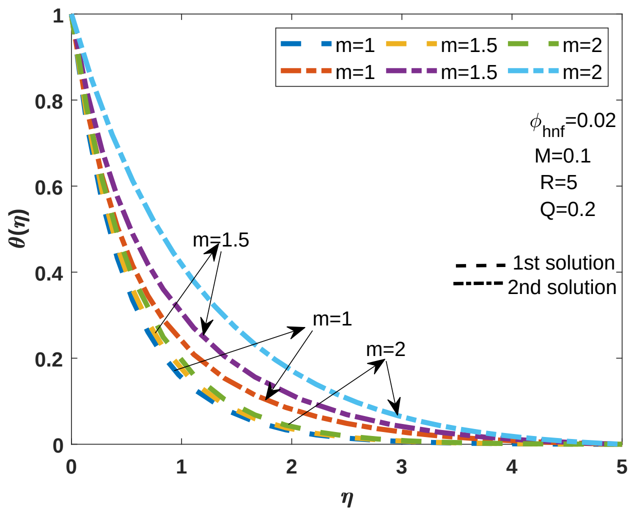

Fig. 9: The effect of m on thermal profile

in the distribution of the fluid temperature due to an increase in the values of variable. Physically, in the case of heat generation, there is a rise in the transfer and thermal spread of the fluids, which raises the temperature of the fluid as well as the temperature and thickness of the boundary layer as the values of the heat source type grow. Figure 9 shows the thermal field of both solutions are boosted, when the non iso-thermal parameter rises.

Skin friction:

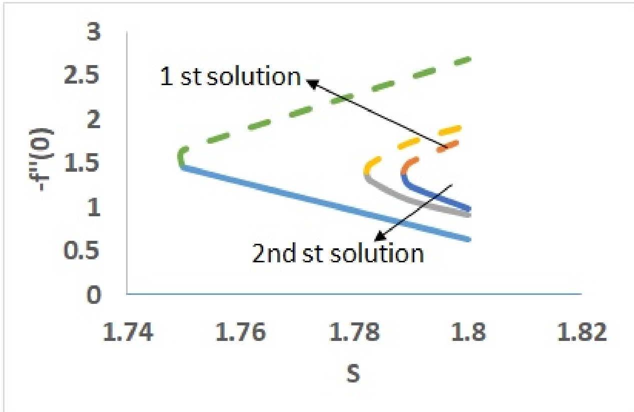

Fig. 10: The effect of S on $Re^{1/2}C_f$ varying $\phi = 0.01, 0.02, 0.03$

Figure 10 depicts the behavior of the skin friction coefficient $f''(0)$ with mass transfer specification S for various values of the volume fraction parameter ϕ_{hnf} over a shrinking sheet. The skin friction coefficient $f''(0)$ increases as the parameter ϕ_{hnf} is increased. For increasing nanoparticle volume fraction of the fluid, the voriticity generation due to shrinking sheet velocity is moderately diminished and thus, with the imposed suction, that vorticity remains confined to the area of a boundary layer. The skin friction values for various parameters, including suction, volume fraction, and magnetic parameters are presented in Table I. The problem of wall friction coefficient of hybrid nanofluid flow model is discussed.

TABLE I: Values of skin friction $Re_x^{-1/2}Cf_x$ with $\lambda = -1$

ϕ_1	ϕ_2	M	S	first solution	second solution
	0.01			1.269915	0.535805
	0.015			1.272911	0.534763
0.011	0.02	0.18	1.9	1.275289	0.533872
	0.025			1.277060	0.533127
	0.03			1.278235	0.532552
		0.1		1.101958	0.719166
		0.2		1.300182	0.502007
0.01	0.01	0.3	1.9	1.423682	0.0362683
		0.4		1.521834	0.253231
		0.5		1.605237	0.162637
			2.1	1.527765	0.417984
			2.0	1.349020	0.538238
0.01	0.01	0.18	1.95	1.241648	0.613441
			1.9	1.101958	0.719166
			1.8	1.986743	-1.997719

heat transfer:

Further, we made comparison with earlier published articles by Grubka and Boba [1] and Ishandar et al. [33] in the absence of thermal radiation, magnetic field and heat

TABLE II: Values of heat transfer $Re_x^{-1/2}Nu_x$ under different values of $\lambda = -1, S = 1.9, and\, \phi_{hnf} = 0.02$

m	R	M	Q	first solution	second solution
0.0	0.0	0.0	0.0	11.11739	11.22672
0.5	1	0.1	0.2	9.514367	10.181195
1.0	1.0	0.1	0.2	10.21489	9.65529
		0.2		8.3008	9.66513
		0.3		8.26772	9.67474
1.0	1.5	0.1	0.2	9.514367	10.18119
	1.3			15.56779	12.81502
	1.5			16.04889	11.71092
1.0	1.0	0.1	0.1	11.97497	9.813295
			0.2	10.21489	9.65529
			0.3	9.28195	9.49327

source to validate the accuracy of the numerical results. The results are in good agreement, as shown in Table III. Table II displays the heat transfer solution of shrinking sheet with various non dimensional parameters

TABLE III: Outputs of$-\theta'(0)$ under various values of Prandtl number through $\lambda = -1, S = M = R = \phi_{hnf} = 0$

m	Pr	Grubka & Bobba [1]	Ishandar et al [33]	Present study
1	0.72	0.8086	0.8086	0.7128
	1	1.0000	1.0000	0.9943
	3	1.9237	1.9237	2.9905

Resource surface methodology

The RSM is a statistical method that is frequently used to establish empirical relationships between several inputs and numerous responses. It is a very effective technique for analyzing a multi-variable and multi-response process since it offers information about the most and least dominating elements that influence the answers. Additionally to modeling and analysis, RSM offers process optimization.

The RSM approach was used in this instance as well to examine the impact of the input values (ϕ_1, ϕ_2,R,Q) on the outcomes (first and second solutions of the Nusselt number), leading to the development of an empirical relationship between them and process optimization. In order to do this, a second-order polynomial was used, which also reveals information about how input elements interact to affect replies. Equation(18) provides the RSM-based second-order mathematical relation that was utilised in this work.

$$Y = \beta_0 + \sum_{i=1}^{p} \beta_i X_i + \sum_{i=1}^{p} \beta_{ii} X_i^2 + \sum_{i=1}^{p} -1 \sum_{j=1}^{p} \beta_{ij} X_i X_j \quad (18)$$

where, β_0 is a constant term, coefficients $\beta_1, \beta_2, \beta_3......\beta_p$ and $\beta_{11}, \beta_{22}, \beta_{33}......\beta_{pp}$ are linear and quadratic terms, while $\beta_{12}, \beta_{13}, ...\beta_{p1}$ are interacting term The complete experimental plan created using the face-centered CCD is shown in Table VI. The development of an empirical model for multi-variable and multi-response issues frequently uses RSM. It can also be successfully applied to process optimization.

$$Response = \beta_0 + \beta_1 A + \beta_2 B + \beta_3 C + \beta_4 D + \beta_5 A^2 + \beta_6 B^2 + \beta_7 C^2 + \beta_8 D^2 + \beta_9 AB + \beta_{10} AC + \beta_{11A} D + \beta_{12} BC + \beta_{13} BD + \beta_{13} CD \quad (19)$$

The fitting model was predicted using a full quadratic polynomial that took into account every component of the response surface. The model was subjected to analysis of variance (ANOVA), which is used to assess the model's relevance as well as the importance of each term in the model.The ANOVA tables IV and V provide the degree of freedom, mean square, and sum of squared deviations for the model as well as for each term.The 95 % confidence interval for RSM means that the model or the term is considered to be significant if the p value (equivalent to the F value) of the term or of the model is determined to be less than 0.05.The figure 11 and 12 shows the residual fitted graph according the first and second solution of Hybrid Nanofluid's flow of nusselt number. Contour plot of this model flow can be represented as figures 13 to 16

TABLE IV: Analysis of variance

Source	DF	Adj SS	Adj MS	F-Value	P-Value
Model	14	29.0055	2.0718	3338.18	$\leq$0.0001
ϕ_1	1	0.0218	0.0218	35.16	$\leq$ 0.0001
ϕ_2	1	0.0185	0.0185	29.88	$\leq$ 0.0001
R	1	27.8795	27.8795	44920.25	$\leq$ 0.0001
Q	1	0.9747	0.9747	1570.53	$\leq$ 0.0001
$\phi_1 * \phi_1$	1	0	0	0.05	0.824
$\phi_2 * \phi_2$	1	0	0	0.05	0.824
R*R	1	0.1016	0.1016	163.78	$\leq$ 0.0001
Q*Q	1	0.0002	0.0002	0.37	0.55
$\phi_1 * \phi_2$	1	0	0	0.02	0.88
ϕ_1*R	1	0.0002	0.0002	0.38	0.545
ϕ_1*Q	1	0	0	0	0.947
ϕ_2*R	1	0.0002	0.0002	0.35	0.565
ϕ_2*Q	1	0	0	0	0.949
R*Q	1	0.0015	0.0015	2.42	0.141
Error	15	0.0093	0.0006		
Lack-of-Fit	10	0.0093	0.0009	*	*
Pure Error	5	0	0		
Total	29	29.0148			

TABLE V: Analysis of Variance

Source	DF	Adj SS	Adj MS	F-Value	P-Value
Model	14	29.0052	2.0718	3339.24	$\leq$ 0.0001
ϕ_1	1	0.0218	0.0218	35.18	$\leq$ 0.0001
ϕ_2	1	0.0185	0.0185	29.88	$\leq$ 0.0001
R	1	27.8792	27.8792	44934.63	$\leq$ 0.0001
4Q	1	0.9747	0.9747	1570.98	$\leq$ 0.0001
ϕ_1*ϕ_1	1	0	0	0.05	0.821
ϕ_2*ϕ_2	1	0	0	0.05	0.821
R*R	1	0.1016	0.1016	163.7	$\leq$ 0.0001
Q*Q	1	0.0002	0.0002	0.38	0.546
ϕ_1*ϕ_2	1	0	0	0.02	0.881
ϕ_1*R	1	0.0002	0.0002	0.38	0.546
ϕ_1*Q	1	0	0	0	0.948
ϕ_2*R	1	0.0002	0.0002	0.35	0.564
ϕ_2*Q	1	0	0	0	0.948
R*Q	1	0.0015	0.0015	2.42	0.141
Error	15	0.0093	0.0006		
Lack-of-Fit	10	0.0093	0.0009	*	*
Pure Error	5	0	0		
Total	29	29.0145			

TABLE VI: Central Composite Design

Run	A	B	C	D	ϕ_1	ϕ_1	R	Q	1st solution	2nd solution
1	-1	-1	-1	-1	0.02	0.02	2	0.2	1.4332	1.4331
2	1	-1	-1	-1	0.04	0.02	2	0.2	1.4844	1.4843
3	-1	1	-1	-1	0.02	0.04	2	0.2	1.4801	1.48
4	1	1	-1	-1	0.04	0.04	2	0.2	1.535	1.5349
5	-1	-1	1	-1	0.02	0.02	4	0.2	3.6212	3.6211
6	1	-1	1	-1	0.04	0.02	4	0.2	3.6869	3.6868
7	-1	1	1	-1	0.02	0.04	4	0.2	3.6819	3.6818
8	1	1	1	-1	0.04	0.04	4	0.2	3.7515	3.7514
9	-1	-1	-1	1	0.02	0.02	2	0.4	1.054	1.0539
10	1	-1	-1	1	0.04	0.02	2	0.4	1.1028	1.1026
11	-1	1	-1	1	0.02	0.04	2	0.4	1.0985	1.0984
12	1	1	-1	1	0.04	0.04	2	0.4	1.1509	1.1508
13	-1	-1	1	1	0.02	0.02	4	0.4	3.2017	3.2016
14	1	-1	1	1	0.04	0.02	4	0.4	3.2665	3.2664
15	-1	1	1	1	0.02	0.04	4	0.4	3.2615	3.2614
16	1	1	1	1	0.04	0.04	4	0.4	3.3303	3.3302
17	-2	0	0	0	0.01	0.03	3	0.3	2.2697	2.2696
18	2	0	0	0	0.05	0.03	3	0.3	2.3935	2.3934
19	0	-2	0	0	0.03	0.01	3	0.3	2.2746	2.2745
20	0	2	0	0	0.03	0.05	3	0.3	2.3886	2.3885
21	0	0	-2	0	0.03	0.03	1	0.3	0.4783	0.4782
22	0	0	2	0	0.03	0.03	5	0.3	4.6805	4.6804
23	0	0	0	-2	0.03	0.03	3	0.1	2.7314	2.7313
24	0	0	0	2	0.03	0.03	3	0.5	1.9171	1.917
25	0	0	0	0	0.03	0.03	3	0.3	2.3307	2.3305
26	0	0	0	0	0.03	0.03	3	0.3	2.3307	2.3305
27	0	0	0	0	0.03	0.03	3	0.3	2.3307	2.3305
28	0	0	0	0	0.03	0.03	3	0.3	2.3307	2.3305
29	0	0	0	0	0.03	0.03	3	0.3	2.3307	2.3305
30	0	0	0	0	0.03	0.03	3	0.3	2.3307	2.3305

Regression Equation

$$\begin{aligned}\text{first solution} = {} & 0.011 + 2.36\phi_1 + 2.17\phi_2 + 0.7192R - 1.524Q - 11.0\phi_1 * \phi_1 - 11.0\phi_2 * \phi_2 \\ & + 0.06085R * R - 0.294Q * Q + 9.5\phi_1 * \phi_2 + 0.385\phi_1 * R - 0.41\phi_1 * Q \\ & + 0.367\phi_2 * R - 0.41\phi_2 * Q - 0.0969R * Q \end{aligned} \tag{20}$$

$$\begin{aligned}\text{second solution} = {} & 0.012 + 2.34\phi_1 + 2.16\phi_2 + 0.7190R - 1.525Q - 10.7\phi_1 * \phi_1 - 10.7\phi_2 * \phi_2 \\ & + 0.06088R * R - 0.291Q * Q + 9.6\phi_1 * \phi_2 + 0.386\phi_1 * R - 0.42\phi_1 * Q \\ & + 0.367\phi_2 * R - 0.41phi2 * Q - 0.0968R * Q \end{aligned} \tag{21}$$

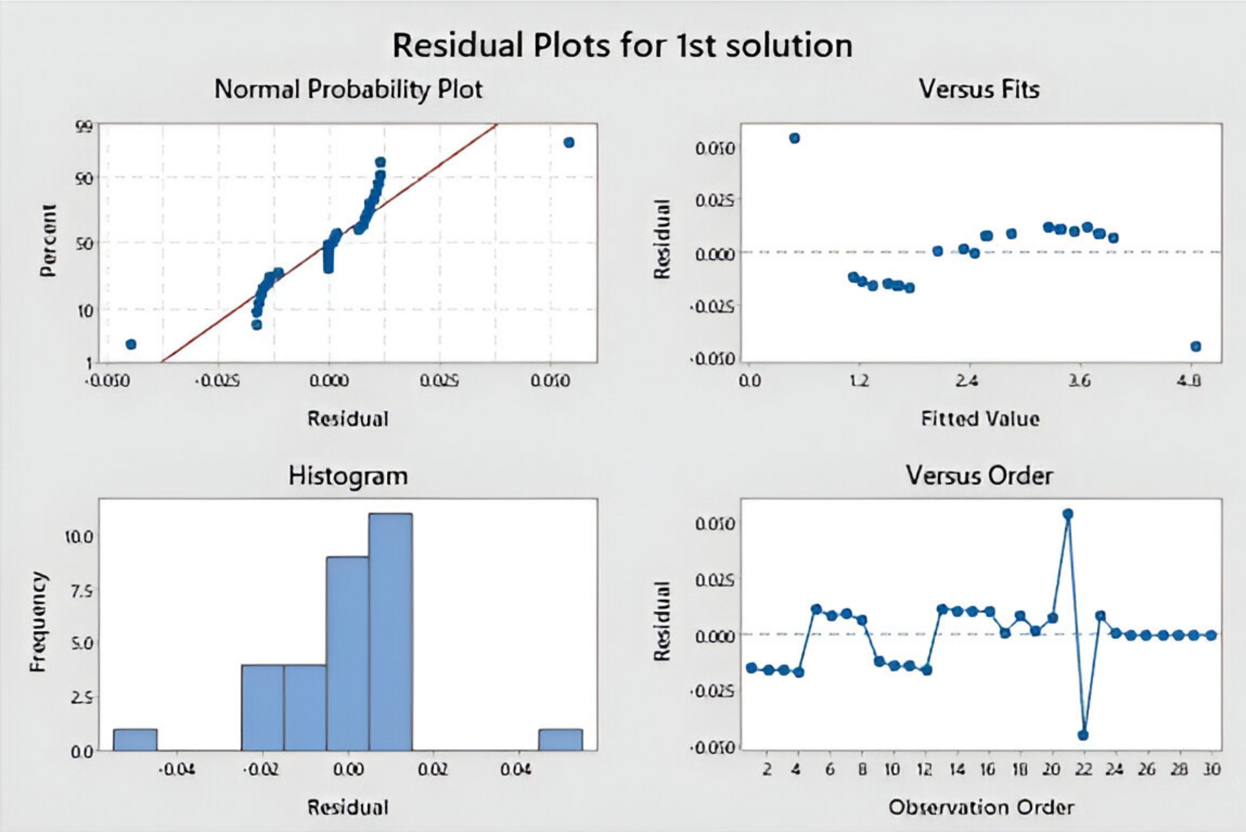

Fig. 11: Residual plot of 1st solution

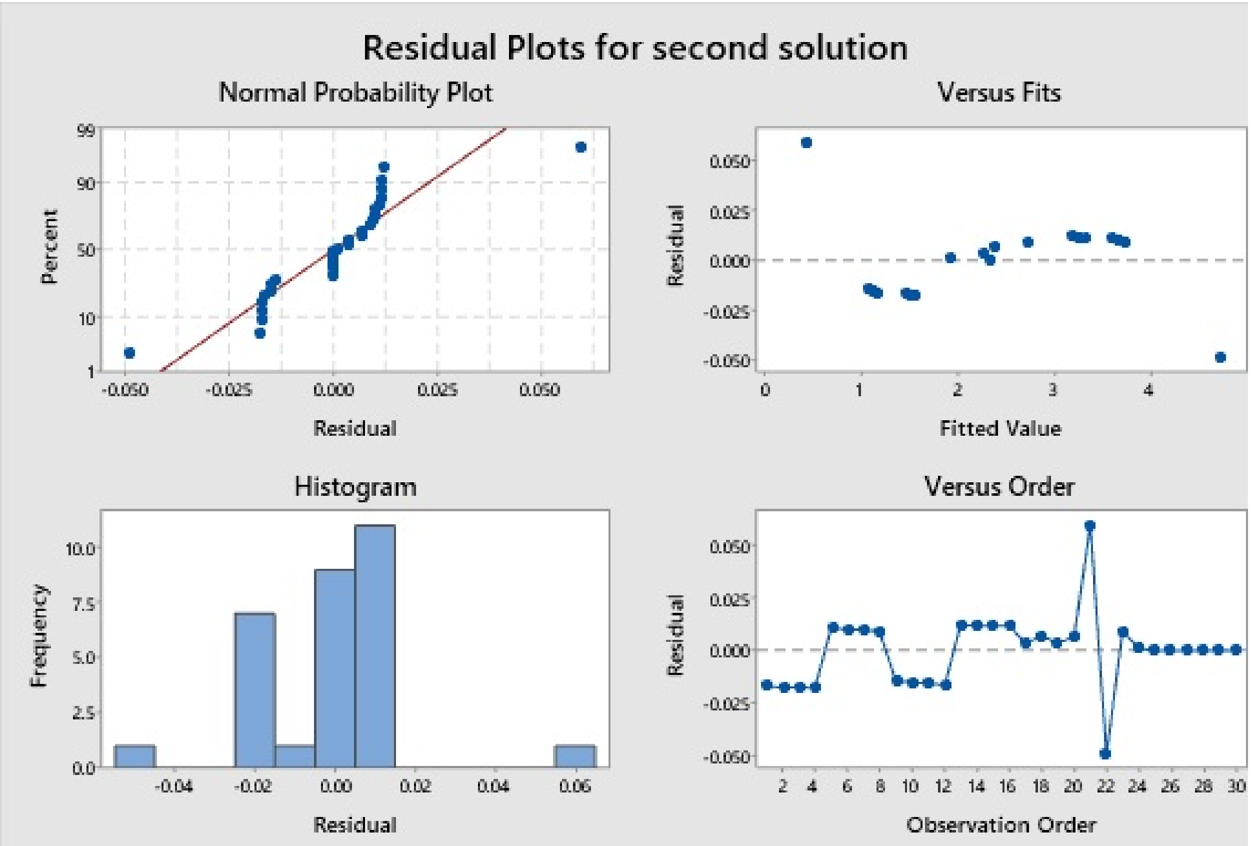

Fig. 12: Residual plot of 2nd solution

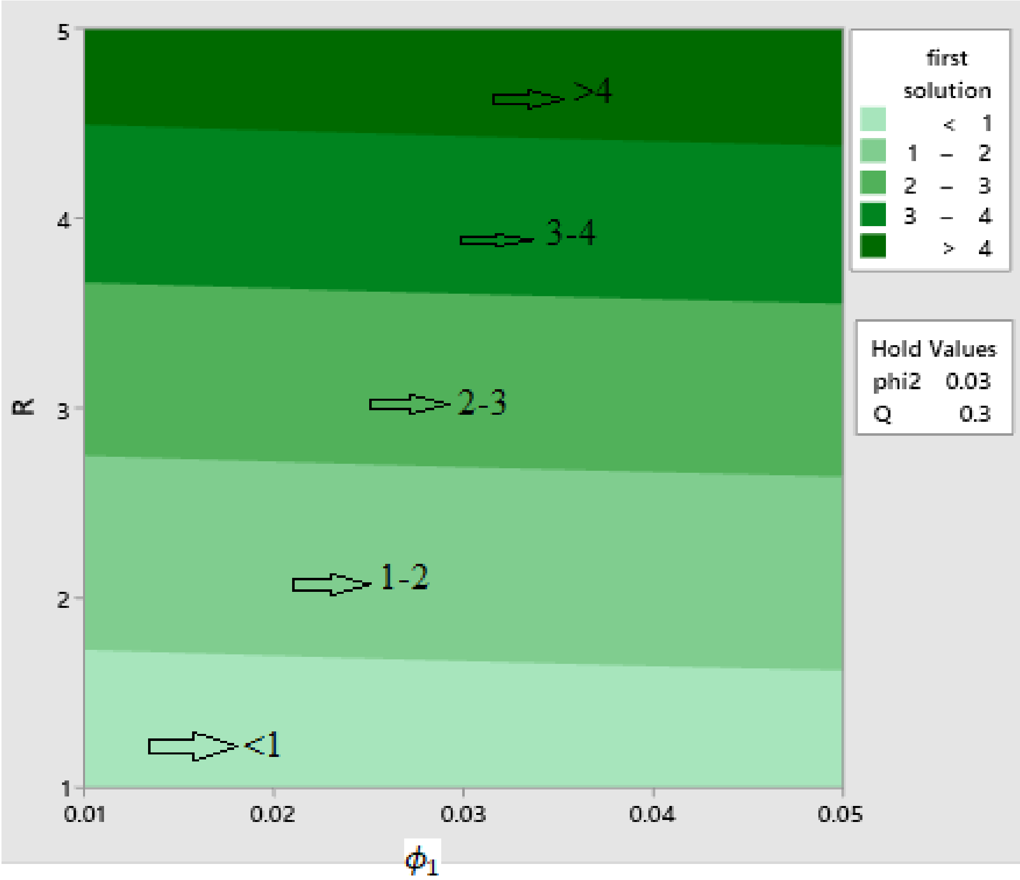

Fig. 13: Contour plot of 1st solution Vs ϕ_1,R

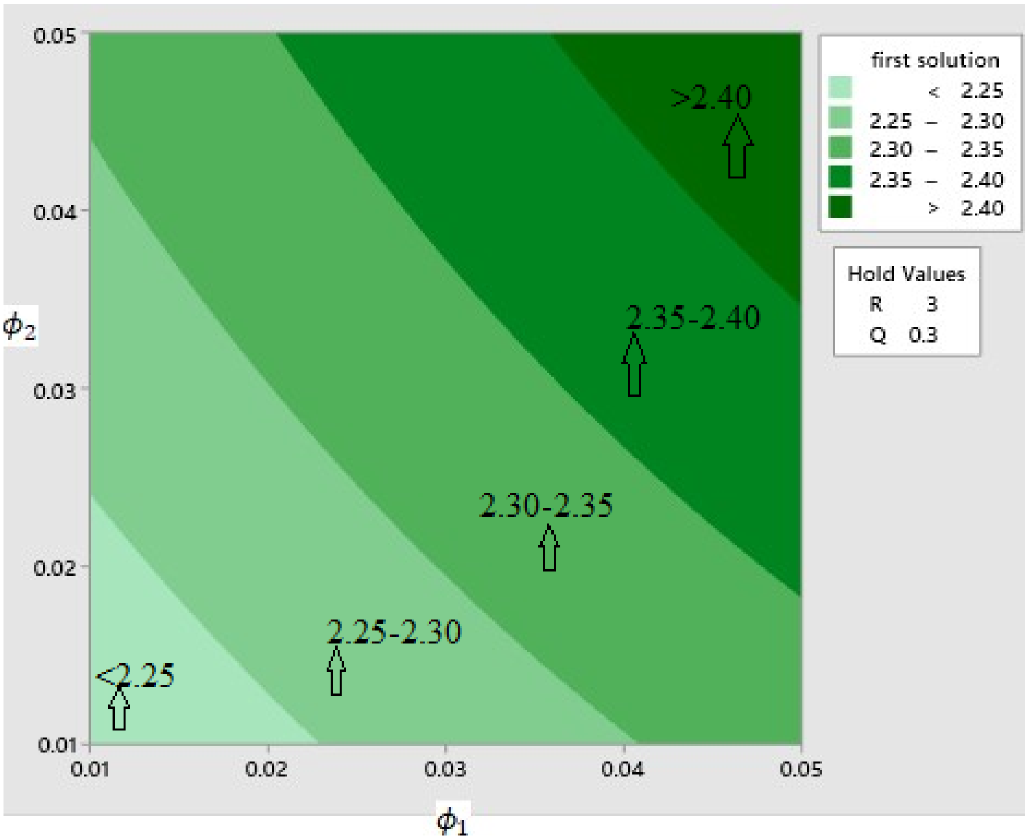

Fig. 14: Contour plot of 1st solution Vs ϕ_1, ϕ_2

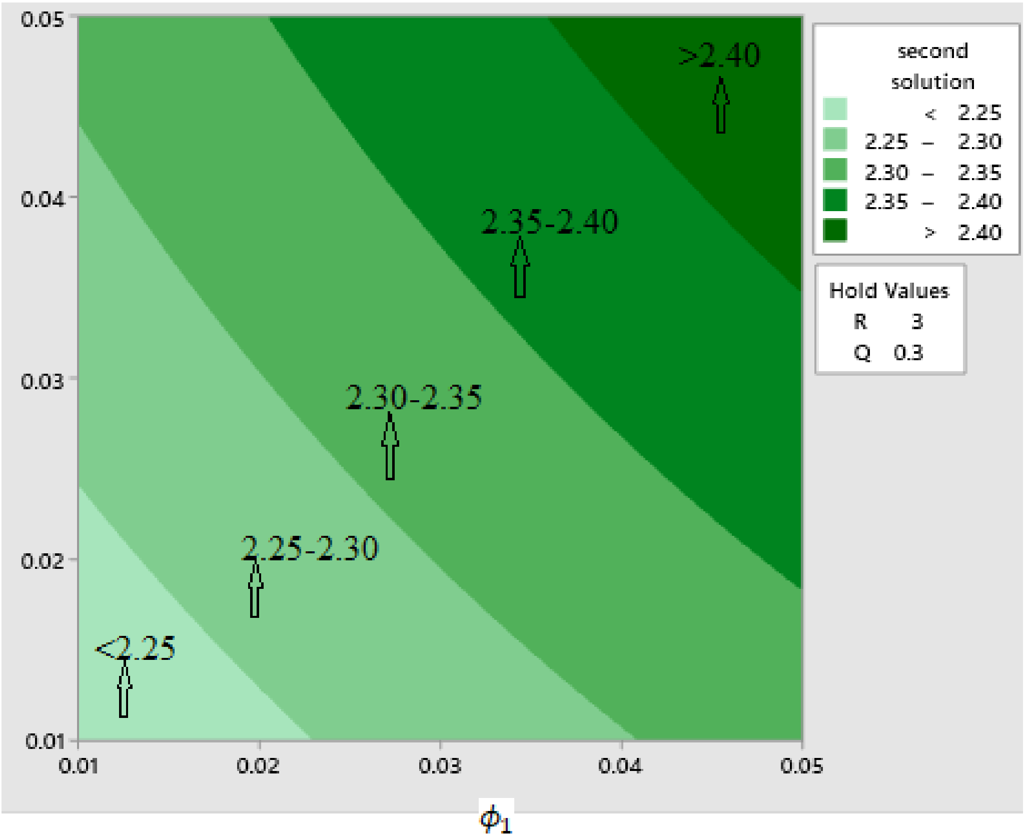

Fig. 15: Contour plot of 2nd solution Vs ϕ_1, ϕ_2

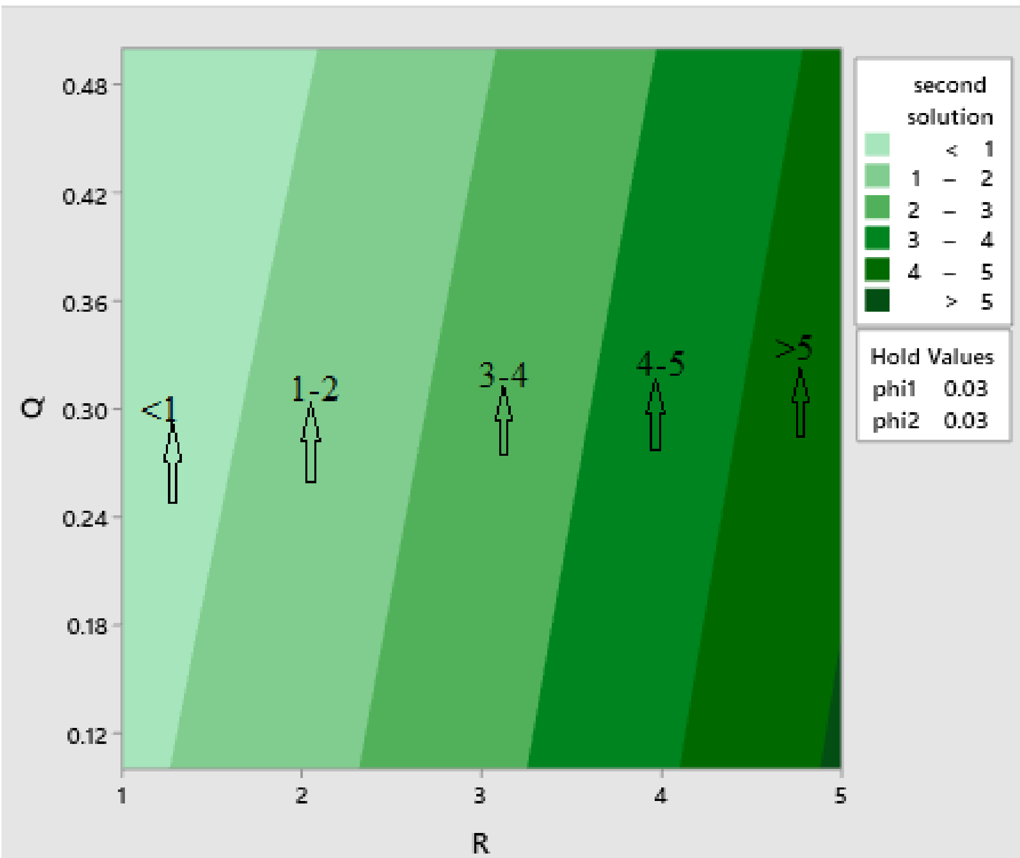

Fig. 16: Contour plot of 2nd solution Vs Q, R

IV. Conclusion

This research paper discusses the skin friction of the MHD hybrid nanofluid over a shrinking surface in the presence of thermal radiation. Furthermore, it investigates the properties of hybrid nanofluid in heat transmission with the impact of a heat source/sink. The established problem with these physical impacts had significant importance. A formal numerical technique is adopted to demonstrate the influence of all physical parameters on the dual velocity and temperature profiles. The conclusions derived from the findings of the current work are summarized as below :

•For both solutions of horizontal velocity, the components are improved with an increase in the nanoparticle volume fraction.

• In the first and second solutions, the velocity distribution reduces with an increase in the values of suction and magnetic parameters.

•It is observed that there is enhancement in the values of ${Re_x^{-1/2}}C_f$ in the first solution with an increasing volume fraction. The influence of different (ϕ_1, ϕ_2) values of the suction parameter (S) is examined. It is noted that higher values of M, R, and Q trend to boost the thermal delineation.

•We involved the careful application of the resource surface approach, which enabled us to investigate the importance of key parameters such as volume fraction, thermal radiation, heat source/sink. Through this meticulous analysis, we aimed to gain valuable insights into their roles and effects within our study, understanding of the phenomena under investigation.

References

[1] L. J. Grubka and K. M. Bobba "Heat Transfer Characteristics of a Continuous, Stretching Surface With Variable Temperature," *Journal of Heat Transfer*, vol. 107, pp. 248-250, 1985.

[2] J. H. Merkin, "On dual solutions occurring in mixed convection in porous medium," *Journal of Engineering Mathematics*, vol. 20, no. 2, pp.171-179, 1986

[3] P. D. Weidman, D. G. Kubitscheck, and A. M. Davis "The effect of transpiration on self-similar boundary layer flow over moving surfaces," *Journal of Engineering Mathematics*, vol. 44, pp. 730-737, 2006.

[4] T. Fang, "Boundary layer flow over a shrinking sheet with power-law velocity,"*International Journal of Heat and Mass Transfer*, vol. 51, pp. 5838-5843, 2008.

[5] F. Tie-Gang, Z. Ji, and Y. Shan-Shan, "Viscous flow over an unsteady shrinking sheet with mass transfer," *Chinese Physics Letters*, vol. 26, no. 1, pp. 014703, 2009.

[6] N. M. Arifin, R. Nazar, and I. Pop, " Viscous flow due to a permeable stretching/shrinking sheet in a nanofluid," *Sains Malaysiana*, vol. 40, no.12, pp. 1359-1367, 2011.

[7] A. M. Rohni, S. Ahmad, A. I. M. Ismail, and I. Pop,"Flow over an unsteady shrinking sheet with suction in a nanofluid," *International Journal of Modern Physics: Conference Series*, vol. 9, pp. 511-519, 2012.

[8] K. Zaimi, A. Ishak,and I. Pop, "Boundary layer flow and heat transfer past a permeable shrinking sheet in a nanofluid with radiation effect," *Advances in Mechanical Engineering*, vol. 4, pp. 340354, 2012

[9] N. Bachok, A. Ishak, R. Nazar, and N. Senu, "Stagnation-point flow over a permeable stretching/shrinking sheet in a copper-water nanofluid," *Boundary Value Problems*, vol. 1, pp. 1-10, 2013.

[10] A. M.Rohni, S. Ahmad, A. I. M. Ismail, and I. Pop, "Flow and heat transfer over an unsteady shrinking sheet with suction in a nanofluid using Buongiorno's model," *International Communications in Heat and Mass Transfer*, vol. 43, pp. 75-80, 2013.

[11] K. Das, "Cu-water nanofluid flow and heat transfer over a shrinking sheet," *Journal of Mechanical Science and Technology*, vol. 28, no. 12, pp. 5089-5094, 2014.

[12] K. Das, "Nanofluid flow over a shrinking sheet with surface slip," *Microfluidics and nanofluidics*, vol. 16, pp.391-401, 2014.

[13] V. B. Awati, and N. M. Bujurke, "Approximate analytical solutions of MHD flow of a viscous fluid on a nonlinear porous shrinking sheet," *Bulletin of the International Mathematical Virtual Institute*, vol. 4, pp. 145-155, 2014.

[14] M. E. H. Hafidzuddin, and R. Nazar, "Numerical solutions of MHD rotating flow and heat transfer over a permeable shrinking sheet," *Science Asia*, vol. 40, no.1, pp.58-62, 2014.

[15] R. D. Ene, M. A. Szabo, and S. Danoiu, "Viscous Flow and Heat Transfer Over a Permeable Shrinking Sheet with Partial Slip," *Mater Plast*, vol. 52, no. 3, pp. 408-412, 2015.

[16] B. Yao, and G. Wu, "Approximate analytical multiple solutions of the boundary layer flow over a shrinking sheet with power-law velocity," *International Journal of Heat and Mass Transfer*, vol. 85, pp.615-619, 2015.

[17] A. S. Dogonchi, and D. D. Ganji, "Investigation of MHD nanofluid flow and heat transfer in a stretching/ shrinking convergent/divergent channel considering thermal radiation," *Journal of Molecular Liquids*, vol. 220, pp. 592-603, 2016.

[18] K. Das, N. Acharya and P. K. Kundu "The onset of nanofluid flow past a convectively heated shrinking sheet in presence of heat source/sink: A Lie group approach," *Applied Thermal Engineering*, vol. 103, pp. 38-46, 2016.

[19] T. Hayat and S. Nadeem, "Heat transfer enhancement with $Ag-CuO$/water hybrid nanofluid," *Results in Physics*, vol. 7, pp. 2317-2324, 2017.

[20] I. Rashid, R. U. Haq, Z. H. Khan and Q. M. Al-Mdallal "Flow of water based alumina and copper nanoparticles along a moving surface with variable temperature," *Journal of Molecular Liquids*, vol. 246, pp. 354-362, 2017.

[21] T. M. Agbaje, S. Mondal, S. S. Motsa and P. Sinbanda, "A numerical study of unsteady non-Newtonian Powell-Eyring nanofluid flow over a shrinking sheet with heat generation and thermal radiation," *Alexandria Engineering Journal* , vol. 56, pp. 81-91, 2017.

[22] T. Thumma, O. A. Beg and A. Kadir, "Numerical study of heat source/sink effects on dissipative magnetic nanofluid flow from a non-linear inclined stretching/shrinking sheet," *Journal of Molecular Liquids*, vol. 232, pp. 159-173, 2017.

[23] K. Vajravelu, K. V. Prasad, C. O. Ng, and H. Vaidya, "MHD flow and heat transfer over a slender elastic permeable sheet in a rotating fluid with Hall current," *International Journal of Applied and Computational Mathematics*, vol. 3, pp. 3175-3200, 2017.

[24] M. Usman and M. Hamid, T. Zubair, R. U. Haq, and W. Wang, "Cu-Al2O3/Water hybrid nanofluid through a permeable surface in the presence of nonlinear radiation and variable thermal conductivity via LSM," *International Journal of Heat and Mass Transfer*, vol. 126, pp. 1347-1356, 2018.

[25] S. S. Ghadikolaei and K. Hosseinzadeh, M. Hatami, and D. D. Ganji, "MHD Boundary layer analysis for micropolar dusty fluid containing Hybrid nanoparticles ($Cu-Al_2O_3$) over a porous medium," *Journal of Molecular Liquids*, vol. 268, pp. 813-823, 2018.

[26] S. S. Ghadikolaei and K. Hosseinzadeh, and D. D. Ganji, "Investigation on ethylene glycol-water mixture fluid suspend by hybrid nanoparticles (TiO_2-CuO) over rotating cone with considering nanoparticles Shape factor," *Journal of Molecular Liquids*, vol. 272, pp. 226-236, 2018.

[27] I. Waini, A. Ishak and I. Pop, "Unsteady flow and heat transfer past a stretching/shrinking sheet in a hybrid nanofluid," *International Journal of Heat and Mass Transfer*, vol. 136, pp. 288-297, 2019.

[28] N. S. Khashi, N. Wahi, A. A. Ghani and K. B. Hamzah "Effect of suction on the MHD flow in a doubly-stratified micropolar fluid over a shrinking sheet," *Mathematical modeling and computing*, vol. 9, no. 1, pp. 92-100, 2022.

[29] N. Japili, H. Rosali and N. Bachok, "MHD stagnation point flow over a stretching or shrinking sheet in a porous medium with velocity slip," *Mathematical Modeling and Computing*, vol. 9, no. 4, pp. 852-832, 2022.

[30] N. H. Norzawary and N. Bachok, F. M. Ali and N. A. Rahmin "Double solutions and stability analysis of slip flow past a stretching/shrinking sheet in a carbon nanotube," *Mathematical Modeling and computing*, vol. 9, no. 4, pp. 816-824, 2022.

[31] S. Dinarvand, M. Yousefi, and A. Chamkha, "Numerical Simulation of Unsteady Flow toward a Stretching/Shrinking Sheet in Porous Medium Filled with a Hybrid Nanofluid ," *Journal of Applied and Computational Mechanics*, vol. 8, no. 1, pp. 11-20, 2022.

[32] M. Sajjad, A. Mujtaba, A. Asghar and T. Y. Ying, "Dual Solutions of Magnetohydrodynamics $Al_2O_3 + Cu$ Hybrid Nanofluid Over a Vertical Exponentially Shrinking Sheet by Presences of Joule Heating and Thermal Slip Condition," *CFD Letters*, vol. 14, no. 8, pp. 100-115, 2022.

[33] I. Waini, A. Ishak and I. Pop "Hybrid nanofluid flow over a permeable Non-Isothermal shrinking surface," *Mathematics*, vol.9, no. 5 pp. 538, 2021.

[34] T. Maranna, U. S. Mahabaleshwar, L. M. Perez, O. Manca,"Flow of viscoelastic ternary nanofluid over a shrinking porous medium with heat

Source/Sink and radiation," *Thermal Science and Engineering Progress*, vol. 40, pp. 101791, 2023.
[35] N. Nithya, B. Vennila, "MHD Nanoliquid Flow Along a Stretched Surface with Thermal Radiation and Chemical Reaction Effects," *Mathematical Modelling of Engineering Problems*, Vol. 9, No. 6, pp. 1704-1710, 2022.
[36] M. Khan, L. Ahmad, M. Yasir, and J. Ahmed, "Numerical analysis in thermally radiative stagnation point flow of cross nanofluid due to shrinking surface: dual solutions," *Applied Nanoscience*, vol. 13, no. 1, pp. 573-584, 2023.
[37] A. B. Vishalakshi, R. Mahesh, U. S. Mahabaleshwar, A. K. Rao, L. M. Perez, and D. Laroze, "MHD Hybrid Nanofluid Flow over a Stretching/Shrinking Sheet with Skin Friction: Effects of Radiation and Mass Transpiration," *Magnetochemistry*, vol. 9, no. 5, pp. 118, 2023.
[38] N. Nithya, B. Vennila, "MHD Nanofluid boundary layer flow over a stretching sheet with viscous, ohmic dissipation," *Mathematical Modeling and computing*, vol. 10, no. 1, pp. 195203, 2023.

NOMENCLATURE

u,v	Velocity components along x and y axis
ϕ_1	Volume fraction of Copper Nanoparticle
ϕ_2	Volume fraction of Aluminium oxide Nanoparticle
hnf	Hybrid nanofluid
nf	Nanofluid
f	Base fluid
R	Thermal radiation
M	magnetic field
m	Non isothermal parameter
S	Suction parameter
λ	Shrinking parameter
ν	Dynamic viscosity
μ	Kinematic viscosity
ρ	Density
k	Thermal conductivity
σ	Electrical conductivity
C_p	Specific heat capacity
T_w	Wall temperature
T_∞	Ambient temperature